Solution structure and backbone dynamics of an N-terminal ubiquitin-like domain in the GLUT4-regulating protein, TUG

M. CRISTINA TETTAMANZI,[1] CHENFEI YU,[2] JONATHAN S. BOGAN,[2] AND MICHAEL E. HODSDON[1]

[1]Department of Laboratory Medicine, Yale University, New Haven, Connecticut 06520-8035, USA
[2]Section of Endocrinology and Metabolism, Department of Internal Medicine, Yale University, New Haven, Connecticut 06520-8020, USA

(RECEIVED October 10, 2005; FINAL REVISION November 30, 2005; ACCEPTED December 7, 2005)

Abstract

The GLUT4-regulating protein, TUG, functions to retain GLUT4-containing membrane vesicles intracellularly and, in response to insulin stimulation, releases these vesicles to the cellular exocytic machinery for translocation to the plasma membrane. As part of our ongoing effort to describe the molecular basis for TUG function, we have determined the tertiary structure and characterized the backbone dynamics for an N-terminal ubiquitin-like domain (TUG–UBL1) using NMR spectroscopy. A well-ordered conformation is observed for residues 10–83 of full-length TUG, and confirms a β-grasp or ubiquitin-like topology. Although not required for in vitro association with GLUT4, the functional role of the TUG–UBL1 domain has not yet been described. We undertook a limited literature review of similar N-terminal UBL domains and noted that a majority participate in protein–protein interactions, generally functioning as adaptor modules to physically associate the overall activity of the protein with a specific cellular process, such as the ubiquitin–proteasome pathway. In consistent fashion, TUG–UBL1 is not expected to participate in a covalent protein modification reaction as it lacks the characteristic C-terminal diglycine ("GG") motif required for conjugation to an acceptor lysine, and also lacks the three most common acceptor lysine residues involved in polyubiquitination. Additionally, analysis of the TUG–UBL1 molecular surface reveals a lack of conservation of the "Ile-44 hydrophobic face" typically involved in ubiquitin recognition. Instead, we speculate on the possible significance of a concentrated area of negative electrostatic potential with increased backbone mobility, both of which are features suggestive of a potential protein–protein interaction site.

Keywords: protein trafficking/sorting; NMR spectroscopy; relaxation measurements; protein structures—new; protein–protein interactions

Supplemental material: see www.proteinscience.org

Reprint requests to: Michael E. Hodsdon, Department of Laboratory Medicine, Yale University, New Haven, CT 06520-8035, USA; e-mail: michael.hodsdon@yale.edu; fax: (203) 688-8704.

Abbreviations: GLUT4, Glucose transporter-4; UBL, ubiquitin-like; UBX, ubiquitin regulatory X; VCP, valosin-containing protein; ASPL, alveolar soft part sarcoma locus; SUMO1, small ubiquitin-related modifier-1; FAF1, Fas-associated factor-1; NMR, nuclear magnetic resonance; 2D, two-dimensional; CSI, chemical shift index; NOE, nuclear Overhauser enhancement; UIM, ubiqitin-interacting motif; UBA, ubiquitin-associated; UEV, ubiquitin conjugating enzyme E2 variant; NZF, Npl4 zinc finger; GST, glutathione-S-transferase; IPTG, isopropyl thiogalactopyranoside; PFG, pulsed-field gradients.

Article and publication are at http://www.proteinscience.org/cgi/doi/10.1110/ps.051901806.

One of the ultimate consequences of insulin action on adipose and muscle cells is the redistribution of GLUT4 glucose transporters to the plasma membrane. Insertion of these transporters into the plasma membrane enhances the uptake of extracellular glucose. GLUT4 recycles continuously between the plasma membrane and intracellular compartments. In the absence of insulin, GLUT4-containing membrane vesicles accumulate intracellularly to form an "insulin-responsive compartment," which is most likely associated with elements of the trans-Golgi network (Bryant et al. 2002). Insulin

accelerates dramatically the movement of these vesicles to the plasma membrane, so as to alter the steady-state distribution of the transporters. The molecular basis for this action has been poorly understood. Recently, using a functional screen to identify proteins that modulate GLUT4 trafficking, Bogan and coworkers discovered and characterized a novel GLUT4-regulating protein, named TUG (Bogan et al. 2003). According to the model they propose, GLUT4 that is endocytosed from the plasma membrane is bound specifically by TUG, which may be recruited from a cytosolic pool. The GLUT4-containing vesicles are then tethered and retained intracellularly by TUG together with other proteins in the absence of insulin. Insulin stimulates the release of tethered GLUT4, allowing the rapid mobilization of glucose transporters to the cell surface.

Similar to many other intracellular proteins, TUG appears to contain a modular array of protein domains, each of which may be associated with an independent and specific molecular function (Fig. 1A). Most notable is the presence of two potential "ubiquitin-like" (UBL) domains, here termed "UBL1" and "UBX." Similar UBL domains have been identified in a startling number of intracellular proteins, where they play critical roles in mediating protein–protein interactions or serve as substrates for protein conjugation reactions (Schwartz and Hochstrasser 2003). In TUG, the first UBL domain comprises residues 10–86 at the N terminus, and the UBX domain is located near the C terminus. UBX refers to the recently identified family of "ubiquitin regulatory X" domains considered to serve as a conserved recognition module for the N-terminal domain of p97/VCP, a AAA ATPase family member that functions as a generic molecular motor in a diversity of cellular processes (Dreveny et al. 2004; Yuan et al. 2004). Figure 1B presents a protein sequence alignment of the TUG UBL domains with those from its likely human homolog, ASPL, as well as with ubiquitin, SUMO1, and the FAF1 UBX domain. Research over the past decade demonstrates that ubiquitin, UBL domains, and UBL conjugation reactions play integral roles in the conserved pathways for vesicle trafficking and sorting. Hence, the presence of these domains in a protein intimately related to trafficking of GLUT4-containing vesicles is consistent with this role. Here, we present the NMR-based solution structure and backbone dynamics of the N-terminal UBL domain and discuss its potential functional role.

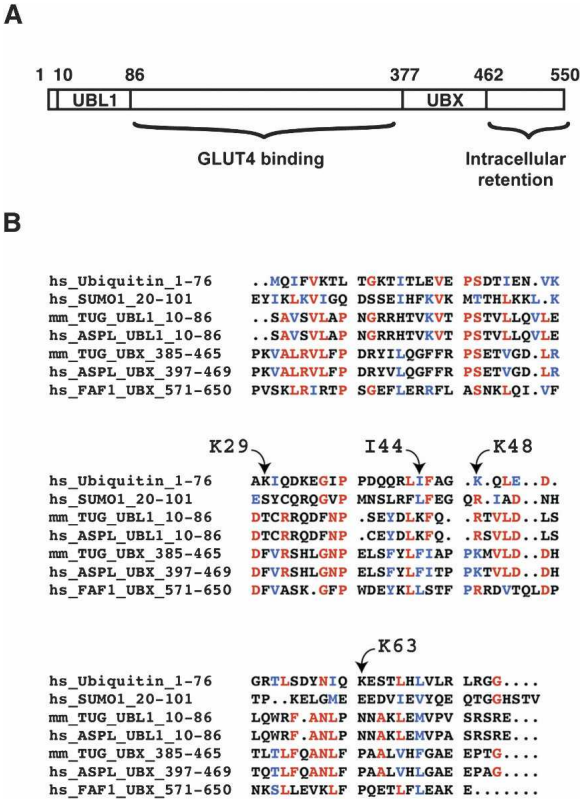

Figure 1. Modular structure of TUG. (*A*) Arrangement of TUG domains identified by sequence similarity searches. Numbering of amino acid residues, from the start codon of the long splice variant, is shown *above* the rectangle representing the TUG sequence (Bogan et al. 2003). The beginning and end of the UBL domains are indicated. *Below* the rectangle, regions implicated in GLUT4 binding and in intracellular retention are indicated. (*B*) Sequence alignment of TUG UBL domains with other ubiquitin-like folds, including those of ubiquitin, SUMO1, UBL domains from ASPL (the likely human homolog of TUG), and the FAF1 UBX domain. Alignments were constructed using T-Coffee (Notredame et al. 2000), and residues were further repositioned by eye. "hs" indicates sequence is from *Homo sapiens*; "mm" indicates *Mus musculus*. The positions of the aligned residues are given in each case. Positions that are identical among the majority of sequences are indicated in red, and those that are conserved are in blue. The locations of the most common lysine residues involved in polyubiquitination, along with Ile-44, are noted in the sequence of ubiquitin.

Results

Resonance assignment

^{1}H, ^{13}C and ^{15}N NMR chemical shift assignments for TUG–UBL1 were established for nearly all backbone atoms (excepting proline amide ^{15}N nuclei) and a majority (>95%) of all side-chain aliphatic and aromatic resonances. However, most side-chain carboxylate (Glu and Asp), amide (Gln and Asn), amines (Lys), and guanidinium (Arg) groups were not assigned. The 2D ^{1}H-^{15}N HSQC spectrum of TUG–UBL1 (Fig. 2) illustrates good dispersion of the amide resonances expected for a protein of this size. In this spectrum, all of the expected backbone amide resonances for residues 2–90 (excepting prolines) are visible and labeled, along with the side-chain ε2 amide for Trp-65. The completeness of the NMR chemical shift assignments for TUG–UBL1

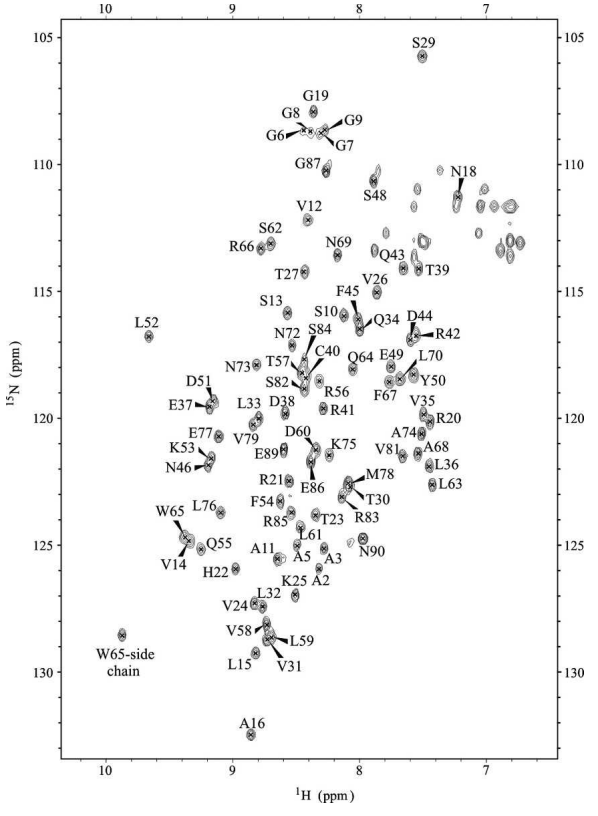

Figure 2. The 2D ^{1}H-^{15}N HSQC NMR spectrum of TUG–UBL1. Backbone amide correlations are labeled for all nonprolyl residues from A2 to N90, along with the side-chain ε2 amide for W65.

aided in the automated interpretation of NOESY correlations detailed below.

Structure determination

Tertiary structures for the TUG–UBL1 domain were calculated using the CYANA 1.0.5 software package (Guntert et al. 1997; Herrmann et al. 2002) and conformational restraints as detailed in Materials and Methods and summarized in Table 1. Although chemical shift assignments had been established for the entirety of residues 1–92 in TUG, the first 10 residues and last eight residues were determined to be entirely structurally disordered according to the CSI and TALOS-based analyses of their chemical shifts, an absence of long-range NOE correlations, and their backbone amide NMR relaxation measurements. Hence, the structure calculations only included residues 10–85 of TUG–UBL1, which were chosen due to their alignment with ubiquitin in Figure 1. In the final ensemble of NMR structures, no distance restraints were violated by >0.3 Å and no dihedral angle restraint was violated by >5°. A superposition of backbone Cα traces for the ensemble is presented in Figure 3A, with average RMSDs (±SD) from the mean structure of 0.18 ± 0.03 Å for the backbone atoms and 0.72 ± 0.05 Å for all heavy atoms. The tertiary structure of TUG–UBL1, depicted as a backbone ribbon diagram in Figure 3B, confirms a β-grasp or ubiquitin-like topology for this domain, consisting of a mixed five-stranded β-sheet in the order 21534, a single

Table 1. *Summary of the structural restraints and conformational statistics for the ensemble*

NOE upper distance restraints	1080
Intraresidue	166
Sequential	345
Medium range (*i*, *i* ± 2–4)	209
Long range (*i*, *i* > 4)	360
Dihedral angle restraints	
Backbone (ϕ and ψ)	115
Side Chain (χ_1)	33
Hydrogen bond restraints[a]	32
Residual NOE violations	
Number >0.3 Å[b]	0
Maximum violation[c]	0.26 ± 0.06 Å
RMS violation[d]	0.015 ± 0.0014 Å
Residual dihedral angle violations	
Number >5°	1 ± 1
Maximum violation	5.77 ± 3.24°
RMS violation	0.84 ± 0.23°
Average backbone RMSD from the mean (residues 13–83), Å	0.18 ± 0.03 Å
Average heavy atom RMSD from the mean (residues 13–83), Å	0.72 ± 0.05 Å

Procheck-NMR vs. 3.5.4 output (residues 10–85) Ramachandran plot statistics	Ensemble of 20 structures	Lowest energy structure
Residues in most favored regions [A,B,L]	1141 (83.9 %)	57 (83.8 %)
Residues in additionally allowed regions [a,b,l,p]	128 (9.4 %)	5 (7.4 %)
Residues in generously allowed regions [~a,~b,~l,~p]	67 (4.9 %)	5 (7.4 %)
Residues in disallowed regions	24 (1.8 %)	1 (1.5 %)
Total number of nonglycine, nonproline residues	1360 (100 %)	68 (100 %)
Stereochemical parameters (standard deviation in degrees)		
Hydrogen bond energy	1.5	1.5
Chi-1 "pooled"[e]	24.5	24.7
Chi-2 *trans* "pooled"[f]	33.4	40.2

[a] Hydrogen bond restraints implemented as a pair of distance restraints from the carbonyl oxygen to both the amide hydrogen and nitrogen of the bonding partner.
[b] Average number of violated restraints per member of the ensemble.
[c] Average value of the maximum violation in each member of the ensemble.
[d] Root-mean-square violation over all violated restraints.
[e] Average standard deviation of the chi-1 angle away from the nearest, most favored conformation.
[f] Average standard deviation of the chi-2 angle away from the *trans* conformation.

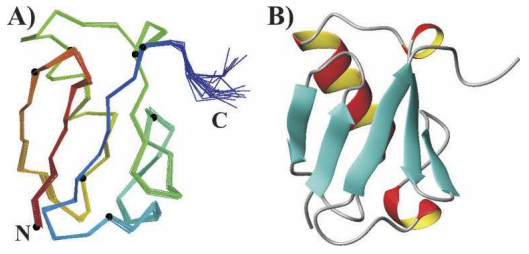

Figure 3. The tertiary structure of TUG–UBL1 as determined by NMR spectroscopy. (*A*) Superposed Cα traces for the ensemble of 20 NMR structures, rainbow-colored from red at the N terminus to blue at the C terminus, prepared using MOLSCRIPT (Kraulis 1991). (*B*) Backbone ribbon diagram for a representative member of the NMR ensemble demonstrating the β-grasp topology conserved within this protein family, prepared using MOLMOL (Koradi et al. 1996).

major α-helix (residues 32–42), and two short helices: one 3_{10}-helix in the loop between strands 4 and 5 (residues 46–49), and a small α-helix (residues 64–69). Thus, the overall organization is $\beta_2\beta_1\alpha(3_{10})\beta_5\beta_3\alpha\beta_4$.

Model-free analysis

The experimental NMR relaxation parameters R_1, R_2, and the heteronuclear ($^1H \rightarrow {}^{15}N$) NOE were measured for a majority of the backbone amides for TUG–UBL1, and are presented at the top of Figure 4. Two distinct components influence the NMR relaxation rates of backbone amide ^{15}N nuclei: the global rotational diffusion of the protein and the internal motions of the NH bond vector relative to the rotational diffusion frame. Model-free theory separates these two components as well as describes the internal motion by amplitude and timescale. NMR relaxation rates are dependent on the spectral densities for the dynamics of the protein backbone and are primarily sensitive to molecular motions on the picosecond-to-nanosecond timescales. Using the model-free formalism to approximate the spectral density functions at the appropriate frequencies, experimental measurement of R_1, R_2, and NOE can be used to characterize internal motions in terms of the generalized order parameter (S^2) and the internal correlation times (τ_e) a parameter which can be related to the amplitude and the effective correlation time for fast internal motions for each amide bond vector, respectively. Whereas R_1, R_2, and NOE are all sensitive to internal motions on a timescale faster than the overall rotational correlation time, the R_2 values can also reflect internal motions occurring on a slower timescale, such as those arising due to chemical exchange or conformational averaging effects. The model-free order parameters (S^2), internal correlation times (τ_e), and chemical exchange rates (R_{ex}) for each backbone N–H bond vector as well as the overall rotational correlation time (τ_m) were derived for TUG–UBL1 and presented in the lower half of Figure 4. The dynamics of TUG–UBL1 is best described by an axially symmetric model of rotational diffusion with overall correlation time τ_m(nsec) of 5.36 and a $D_{ratio} = D_{par}/D_{per}$ of 0.82. The internal mobilities of individual residues are illustrated in Figure 4 by a combination of variations in S^2, which range from 0 to 1 for fully unrestricted to fully restricted motions, respectively, and by the presence of conformational exchange terms ($R_{ex} > 1$), indicating slower timescale internal dynamics on the microsecond-to-millisecond timescale. Examination of the order parameters (S^2 values) for TUG–UBL1 indicates that there are no extended regions of high mobility within the protein, outside of the unstructured N and C termini, which display significantly decreased NOE values. For the remainder of the protein sequence, NOE values for residues 11–82 were found to be on average 0.716 ± 0.06. Order parameters were >0.8 for all remaining residues except for 27, 31, 43, 56, 58, 77, 78, and 83. Of note, a low-order parameter and a high conformational exchange term (R_{ex}) were observed for residue R56 in the loop between β^3 and β^4. This residue is analogous to K48 in ubiquitin, the most common site for covalent attachment of ubiquitin monomers to generate polyubiquitin chains.

Discussion

The NMR structure presented here confirms an N-terminal "ubiquitin-like" domain in the GLUT4-trafficking protein TUG, corresponding to residues 10–85 of the full-length sequence. UBL domains are found in a startling number of intracellular proteins where they play a critical role in mediating protein–protein interactions and serve as substrates for protein conjugation reactions (Schwartz and Hochstrasser 2003). The functional role of TUG's N-terminal UBL domain has not yet been determined. Previous work demonstrates that it is not required for in vitro association of TUG and GLUT4 (Bogan et al. 2003). As N-terminal UBL domains have been identified in many multidomain proteins, we reviewed their descriptions in the literature in order to develop hypotheses about TUG–UBL1's potential physiologic role. Summarized in Table 2 are known biological functions for a listing of N-terminal UBL domains, which was largely based on the excellent phylogenetic analysis of the ubiquitin superfamily by Larsen and Wang (2002). Of those domains experimentally investigated thus far, a large number are believed to interact directly with proteasomal components (most frequently the Rpn10/S5a polypeptide in the 19S regulatory subunit). By physically associating the activities of the

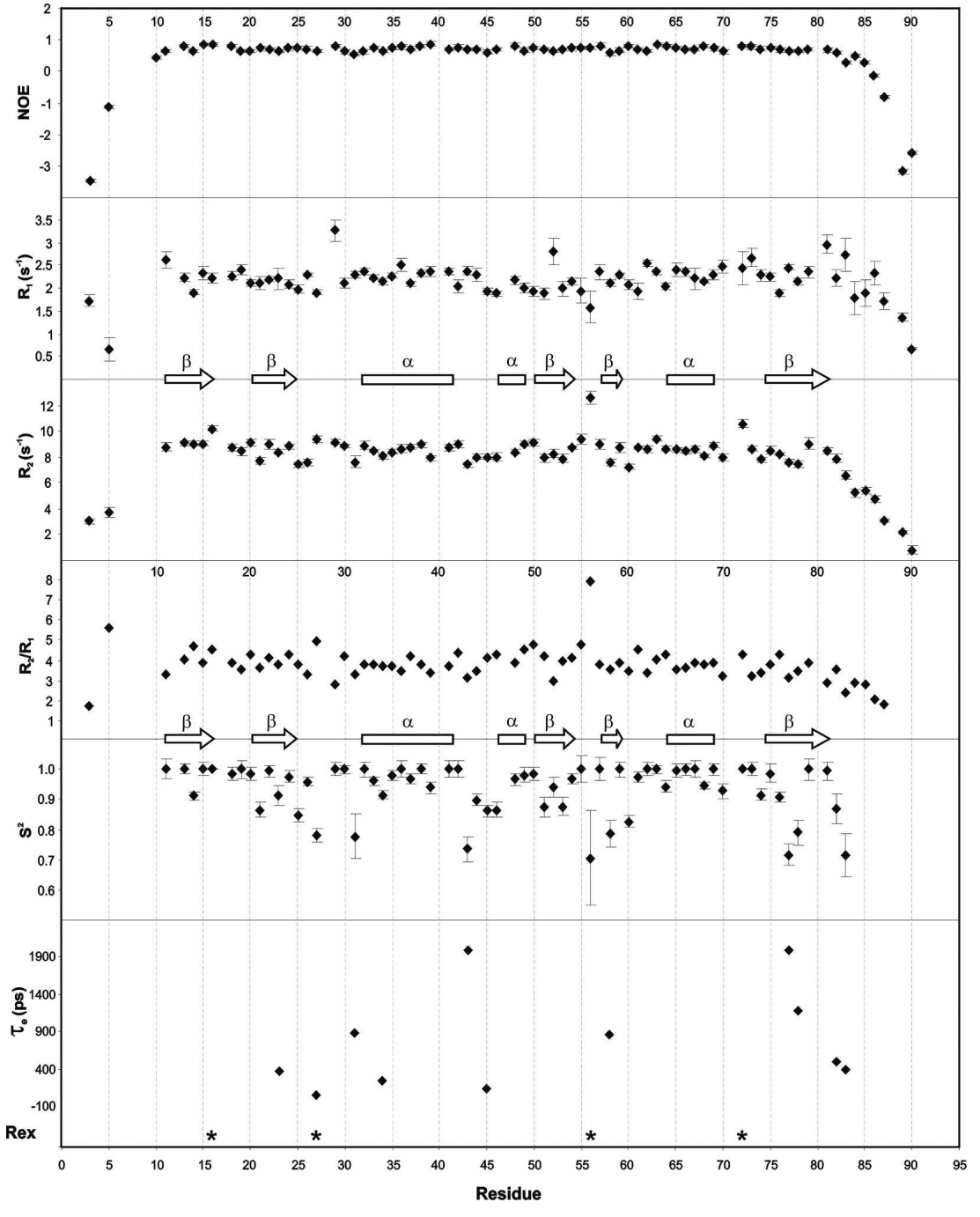

Figure 4. The ^{15}N NMR relaxation data and corresponding model-free motional parameters for TUG–UBL1 are plotted along the primary sequence, with the approximate location of secondary structure elements noted. The location of four residues displaying significant conformational exchange (R_{ex}) terms during model-free analysis are noted by asterisks at the *bottom* in the plot of τ_e values.

C-terminal portions of these proteins with the ubiquitin–proteasome pathway, these N-terminal UBL domains generally function as adaptor modules. With rare exception, they do not participate in covalent conjugation reactions analogous to ubiquitin-like protein modifiers, such as ubiquitin, SUMO, NEDD8, etc. In consistent fashion, TUG–UBL1 lacks the characteristic C-terminal diglycine ("GG") motif required for enzymatic conjugation of the protein to an acceptor lysine. As well, none of the three most common acceptor lysine residues involved

Table 2. *Review of N-terminal UBL domains in modular proteins*

Protein family (pseudonyms and homologs)	Function of the full-length protein	Function of the N-terminal UBL domain	References
Dsk2p (Chap1)	Binds polyubiquitinated proteins. Possible role as an adaptor in the ubiquitin–proteasome pathway	Interacts directly with the 26S proteasome, most likely through Rpn10 (S5a) of the 19S regulatory subunit	(Funakoshi et al. 2002)
Rad23p (HHR23)	Mediates delivery of ubiquitinated substrates to the proteasome; function similar to Dsk2p	Interacts directly with the 26S proteasome, most likely through Rpn10 (S5a) of the 19S regulatory subunit	(Fujiwara et al. 2004; Bazirgan and Hampton 2005)
Mif1 (Herp)	Trans-ER membrane protein that may function to link the cytosolic "unfolded protein response" with ER-associated degradation (ERAD) pathway	Hypothesized to associate with Rpn10 (S5a) of the 19S regulatory subunit of the 26S proteasome, thereby translocating it to the ER-membrane	(van Laar et al. 2001, 2002)
Parkin (Ariadne)	E3 ubiquitin ligase	Binds to Rpn10 (S5a) of the 19S regulatory subunit of the 26S proteasome	(Sakata et al. 2003; Tanaka et al. 2004a)
hPLIC proteins (ubiquilin-1 and 2)	Binds polyubiquitinated proteins; possible role as an adaptor in the ubiquitin–proteasome pathway	Interacts with components of the 20S and 26S proteasome complexes	(Kleijnen et al. 2000; Ko et al. 2004)
NUB1	Associates with NEDD8, FAT10, and UbC1 and functions as an adaptor for interaction with the proteasome and an unidentified ubiquitin hydrolase	Hypothesized to interact directly with components of the proteasome	(Hipp et al. 2004; Tanaka et al. 2004b)
UBP6	A member of the "USP" (ubiquitin-specific protease) class of deubiquitinating enzymes	Interacts directly with the 26S proteasome, most likely through Rpn1 of the 19S regulatory subunit	(Guterman and Glickman 2004)
A1Up	Binds to polyubiquitinated proteins, ataxin-1, and the proteasome	Interacts directly with the 26S proteasome, most likely through Rpn10 (S5a) of the 19S regulatory subunit	(Riley et al. 2004)
BAG proteins	Involved in regulation of apoptosis; appear to serve as cochaperones for Hsp70	Interacts directly with proteasome complexes; note that the UBL domain is not always purely N-terminal	(Alberti et al. 2003)
MNSFβ (Fau, hNSF)	Comprises a UBL fused to the S30 ribosomal protein; involved in immune regulation	Conjugated to intracellular proteins as a ubiquitin-like protein modifier; also noncovalently binds to histone 2A	(Nakamura and Tanigawa 2005)
Scythe (Bat3)	Regulator of apoptosis	Unknown	(Thress et al. 1998; Wu et al. 2004)
ISG15 (UCRP)	A tandem pair of UBL domains, which are conjugated to cellular proteins after IFN-α/β stimulation	Unknown; conjugation only involves the C-terminal UBL domain	(Zhao et al. 2004; Narasimhan et al. 2005)
FAT10	A tandem pair of UBL domains capable of mediating ubiquitin-independent proteasomal degradation	Possibly involved in binding to NUB-1L; conjugation only involves the C-terminal UBL domain	(Hipp et al. 2004, 2005)
GDX	A tandem pair of UBL domains with unknown function	Unknown	(Toniolo et al. 1988)

in polyubiquitination (represented in ubiquitin as K29, K48, and K63) are conserved in UBL1. Hence, it appears very unlikely that this domain functions as a traditional ubiquitin-like protein modifier. It is more likely that TUG–UBL1 participates in a protein–protein interaction, possibly with one of the growing list of ubiquitin-binding domains (UIM, UBA, CUE, UEV, NZF, etc.) (Di Fiore et al. 2003; Hicke et al. 2005). We do not expect for TUG to participate in the ubiquitin–proteasome pathway as has been observed for a majority of the N-terminal UBL domains reviewed here, although the current results may suggest an intriguing avenue for future study. Instead, it seems plausible that TUG–UBL1 functions similar to that of an adaptor module to couple the GLUT4-tethering activity of TUG to another, yet unidentified, cellular process.

As a first step in exploring the potential functional role of the TUG–UBL1 domain, we analyzed the molecular properties of the UBL1 tertiary structure for features suggestive of a protein–protein interaction site. The structural interactions between ubiquitin and a number of ubiquitin-binding motifs have been described (Hicke et al. 2005), all of which recognize a conserved hydrophobic surface patch on ubiquitin. A highly conserved and key residue in this interaction is Ile-44, which is located in the middle of β-strand 3. The analogous residue in TUG–UBL1 is Lys-53 according to both the sequence alignment and the tertiary structure, which dramatically changes the physicochemical properties of the protein surface in this area (see Fig. 6B, below). A secondary, conserved hydrophobic residue in ubiquitin frequently recognized by ubiquitin-binding motifs, Leu-8, is also not conserved in TUG–UBL1. Hence, the previously described, canonical recognition interface on ubiquitin does not appear to exist in TUG–UBL1, at least not in the same biophysical form. It is more likely that an alternative and possibly novel binding interaction will be identified for this domain. In Figure 5, we present views of the electrostatic charge distribution on the surface of UBL1 as calculated by MOLMOL (Koradi et al. 1996). The largest fraction of the surface area including the exposed face of the major β-sheet, depicted on the lower left of Figure 5A, contains distributed patches of positively charged residues. However, we note a smaller contiguous surface area concentrated with negative electrostatic potential, visible on the upper right of Figure 5A and continuing onto the opposite side of the protein (Fig. 5B), which includes the entire length of the long α-helix. Although purely speculative at this point, these patterns of electrostatic charge on the surface of TUG–UBL1 may play a direct role in protein–protein interactions, as has previously been demonstrated for a variety of

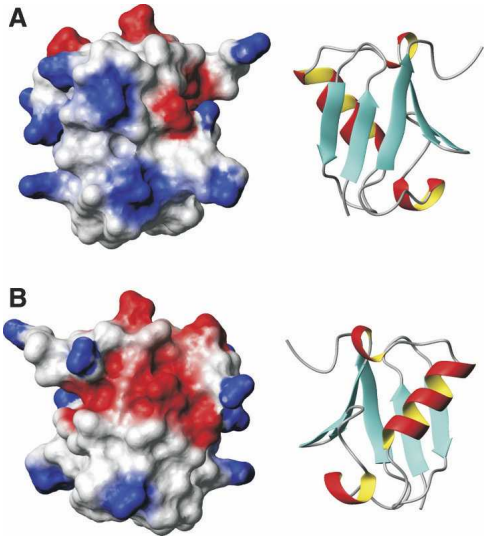

Figure 5. Electrostatic potential mapped onto the molecular surface of the TUG–UBL1 tertiary structure, with coloring in shades of red representing negative potential (q/d, charge per distance) from –5.5 to –1.5 and shades of blue representing positive potential from 1.5 to 5.5, as calculated using MOLMOL (Koradi et al. 1996). Two orientations are shown, with *A* matching the orientation in Figure 3 and *B* rotated by 180°. For clarity, a backbone ribbon diagram corresponding two each orientation is displayed on the *right* of each.

ubiquitin homologs (Liu et al. 1999; Yuan et al. 2001; Wu et al. 2002; Lytle et al. 2004; Ding et al. 2005; Gao et al. 2005).

Another molecular feature commonly associated with protein interaction sites is structural disorder (Farrow et al. 1994; Fushman et al. 1994; Yu et al. 1996; Hodsdon and Cistola 1997; Cheetham et al. 1998; Yuan et al. 1999; Ishima and Torchia 2000; Zuiderweg 2002; Sharrow et al. 2003; Křížová et al. 2004). In the absence of their ligand, protein binding sites often display increased conformational mobility and flexibility in aqueous solution that subsequently become more rigid upon association with ligand. Our analysis of backbone dynamics for UBL1 based upon NMR relaxation revealed a number of residues with increased mobility on both faster (psec and nsec) and slower (μsec to msec) timescales. Figure 6A maps residue-specific differences in structural mobility onto a backbone ribbon diagram of UBL1. Variations in fast timescale motions are represented by shading from blue to red for S^2 values from 1.0 to 0.7, respectively. Additionally, the side chains for four residues with significant contributions due to conformational exchange (R_{ex}) in their transverse (R_2) relaxation rates, representative of slower timescale dynamics, have been noted. A majority of the protein backbone is well ordered with S^2 values >0.9 and an absence of conformational exchange. Nearly all residues with relatively

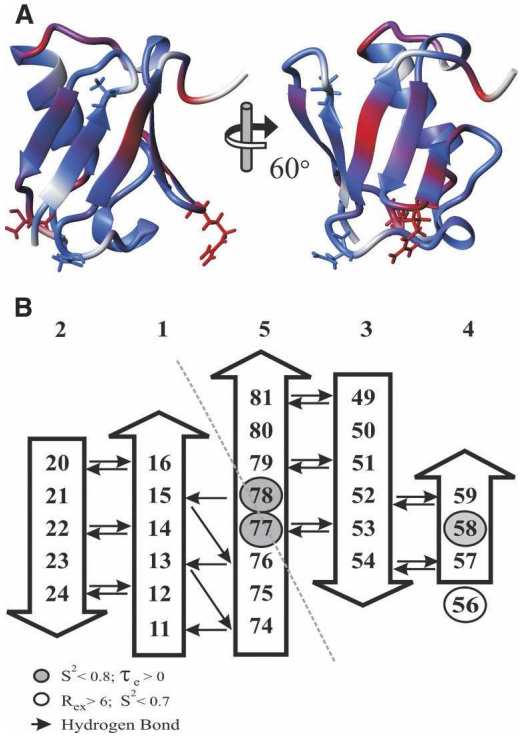

Figure 6. Backbone dynamics of TUG–UBL1. (*A*) Order parameters (S^2) are mapped onto a backbone ribbon diagram with coloring from red to light blue for S^2 values from 0.7 to 1.0, respectively. Prolines and degenerate residues are colored in gray. Side chains are shown for the four residues requiring conformational exchange (R_{ex}) terms during the model-free analysis, with coloring according to S^2 values. (*B*) Hydrogen bonding patterns in the β-sheet with arrows pointing from the amide to the carbonyl. Three residues with S^2 values <0.8 are denoted by the shaded circles. Although formally not a part of the β-sheet, R56 displays a large R_{ex} and low S^2 value, and is also noted by an open circle. As discussed in the text, the β-sheet is fragmented into two subsections (2–1–5 and 5–3–4), denoted by a dashed gray line.

lower S^2 values are found within the loops and turns between secondary structural elements, with the exception of three residues discussed further below. We note a general concentration of mobile residues along the top and the rightward face of UBL1, as oriented on the left side of Figure 6A. After a 60° rotation along the vertical axis (right side of Fig. 6A), this region is better visualized and can be seen to comprise β-strands 5–3–4, the loop after the long α-helix, and the unstructured C terminus. Last, we note significant overlap between this concentration of residues displaying increased conformational mobility and the patch of negative electrostatic charge in Figure 5, both of which may be associated with a potential protein interaction site.

As noted above, although a majority of the β-sheet is well ordered with S^2 values >0.9 and an absence of conformational exchange terms, three residues demonstrated increased fast timescale dynamics with S^2 values <0.8. In order to better understand the origin of these isolated increases in mobility, we analyzed the location of these residues within the pattern of hydrogen bonds for the β-sheet (Fig. 6B). We note two divided hydrogen bonding networks consistent with two adjacent "mini" β-sheets, comprising strands 2–1–5 and 5–3–4. β-Strand 5 is divided nearly equally between the two substructures, with its N-terminal portion contributing to one sheet and its C terminus to the other. Note that within the TUG–UBL1 tertiary structure, the natural left-handed twist along the β-sheet is exaggerated at this division, resulting in a nearly perpendicular orientation between the two proposed mini-sheets. Interestingly, the two residues within β-strand 5 with increased backbone dynamics lie at the interface between these two divided mini-sheets, which may represent a flexible joint to allow a degree of mobility between them. There is also one mobile residue in the shorter fourth β-strand that is likely related to its apparent lack of hydrogen bonding. It is interesting to note that the traditional Ile-44 hydrophobic interaction interface in ubiquitin, discussed above, corresponds closely to the 5–3–4 mini-sheet, for which we observe these localized increases in backbone mobility. As the biological function of TUG and its N-terminal UBL domain is explored further in future studies, it will be interesting to investigate the importance of this structural region.

Materials and methods

NMR sample preparation

cDNA corresponding to residues 1–92 of the full-length TUG protein sequence from *Mus musculus* was subcloned into a modified version of the pGEX-2T bacterial expression plasmid ("pGEX-KG"), and TUG–UBL1 was expressed in the BL21(DE3) *Escherichia coli* strain as a fusion protein with glutathione *S*-transferase (GST). Bacterial cultures were grown at 37°C in either ^{15}N or $^{13}C,^{15}N$ isotope-enriched bacterial growth media (Spectra Stable Isotopes) containing 150 μg/mL ampicillin until the cell density reached A_{600} = 0.6. Protein expression was induced by the addition of isopropyl-β-D-thiogalactopyranoside (IPTG) to a final concentration of 1 mM, and allowed to express for 4–6 h at room temperature. GST–UBL1 was purified from the soluble phase of the cell lysate with glutathione-Sepharose (Amersham Biosciences) and subsequently digested with 10 units/mL thrombin (Amersham Biosciences). Highly purified TUG–UBL1 was separated from GST (along with any remaining uncleaved fusion protein) using glutathione-Sepharose and exchanged into 20 mM NaCl and 20 mM potassium phosphate buffer at pH 7.4. Protein concentration was quantified by UV absorption spectroscopy in 6 M guanidine hydrochloride with absorptivity estimated from the protein sequence. NMR samples contained the above solution conditions, 0.75 mM TUG–UBL1, along with 5% D_2O, 0.05% NaN_3, and 10 μM each of the protease inhibitors PMSF (Sigma) and leupeptin and pepstatin (Calbiochem).

NMR resonance assignments

All NMR experiments were collected at 25°C on a Varian INOVA 600 MHz spectrometer and a "room temperature," 5 mm, triple resonance (HCN) probe equipped with triple-axis (XYZ) pulsed magnetic field gradients (PFGs). All NMR spectra were acquired using pulse sequences from the Varian BioPack user library and processed using NMRPipe (Delaglio et al. 1995). Sequential backbone and aliphatic side-chain assignments were determined by manual analysis of two-dimensional (2D) ^{1}H-^{15}N HSQC, ^{1}H-^{13}C HSQC and three-dimensional (3D) HNCO, HN(CA)CO, HNCACB, HN(CO)CA, HCACO, HCC(CO)NH, ^{15}N-TOCSYHSQC and HCCH-TOCSY NMR experiments collected using ^{13}C,^{15}N-labeled TUG–UBL1. Methionine Hε and Cε resonances for residues 3 and 80 were assigned by correlation to their Cβ chemical shifts in a LRCC NMR spectrum (Bax et al. 1994). Aromatic resonances were assigned using a combination of a 2D ^{1}H-^{13}C HSQC and 3D ^{13}C-NOESYHSQC NMR spectra centered on the aromatic carbons. Stereospecific assignment of 33 β-methylene protons were based on the relative values of the $^{3}J_{N,HB}$ and $^{3}J_{CO,HB}$ coupling constants and the relative intensities of intraresidue Hα–Hβ NOEs, derived from analyses of 3D HNHB, HN(CO)HB, and ^{13}C-NOESYHSQC NMR experiments, respectively. NMR chemical shift assignments for TUG–UBL1 have been deposited in the BioMagResBank (BMRB) with the accession number 6761.

Identification of conformational restraints and structure determination

Backbone ϕ and ψ torsion angle restraints were calculated from patterns of backbone atom chemical shifts using the CSI (Wishart and Sykes 1994) and TALOS (Cornilescu et al. 1999) software packages. Stereospecific assignment of β-methylene protons, detailed above, also resulted in 33 restraints on the χ1 torsion angles for these residues. NOE correlations between nearby protons were identified in 4D ^{13}C,^{15}N-HMQCNOESYHSQC and 3D ^{15}N-NOESY HSQC, ^{13}C-NOESY HSQC (aromatic), and ^{13}C-NOESY HSQC (aliphatic) NMR spectra. All 3D NOESY spectra were extensively analyzed and peak-picked manually using Sparky (D.G. Kneller and T.D. Goddard, University of California, San Francisco); the single 4D NOESY spectrum was visually inspected and subjected to automated peak picking using nmrView (Johnson and Blevins 1994). NOESY peak lists containing chemical shift and intensity data along with all the dihedral angle restraints were input into CANDID for automated interpretation of NOE distance restraints and calculation of preliminary structural ensembles. A limited number of manual NOE interpretations were based on symmetry-related 3D NOE cross-peaks and consideration of the predicted secondary structure. Inclusion of these manual restraints improved convergence during CANDID calculations. All frequently violated NOEs were inspected manually for accuracy and corrected, as necessary, during an additional five rounds of manual and automated NOE interpretations, which ultimately led to a self-consistent set of distance restraints and well-defined tertiary structures. Hydrogen bonds were iteratively identified during the later stages of structure determination based upon the consistent proximity of hydrogen bonding partners in the calculated ensembles and also agreement with expected secondary structure relationships. Hydrogen bond restraints were initially implemented as pairs of loose distance restraints but were eventually tightened for the final rounds of structure calculations to restrain the distance between the donor hydrogen and the acceptor oxygen to 1.8–2.0 Å and the distance between the corresponding amide nitrogen and the acceptor oxygen to 2.7–3.0 Å. The final series of structure calculations were performed by CYANA using the structural restraints summarized in Table 1. Upper bounds for all NOE distance restraints were automatically calibrated by CYANA and adjusted for nonstereospecifically assigned aromatic, methylene, and methyl protons using the method described originally for DYANA (Guntert et al. 1997) and detailed by Guntert (1998). Starting with randomized conformations of the TUG–UBL1 sequence and after an initial brief minimization, simulated annealing began with 5000 steps of molecular dynamics at high temperature, followed by 35,000 dynamics steps during the cooling phase of annealing and a final 10,000 steps of conjugate gradient minimization. Generally, 50 structures were independently calculated, and the 20 structures with the lowest target function values were retained as the final ensemble. Visualization and graphic rendering of the protein structures for the figures was performed using MOLMOL (Koradi et al. 1996). Atomic coordinates for TUG–UBL1 and structural constraints have been deposited in the Protein Data Bank with PDB identifier 2AL3.

NMR relaxation measurements

Pulse sequences for measurement of NMR relaxation rates and the steady-state ^{1}H ^{15}N NOE incorporated sensitivity enhancement, water flip-back pulses, and coherence selection via PFGs (Farrow et al. 1994). For determination of R_1 relaxation rates, NMR experiments were serially repeated with time delays of 100 (×2), 200, 300, 400, 500 (×2), 750, 1000 (×2), 1500 (×2), and 2000 msec, and for determination of R_2, experiments were serially repeated with delays of 10 (×2), 30 (×2), 50 (×2), 70, 90 (×2), 130, 190 (×2), and 250 (×2) msec. The steady-state NOE experiment was performed with and without a 3-sec saturation period to allow buildup of the NOE. Individual increments were separated by a 1-sec recycle delay during determination of R_1 and R_2 relaxation rates, while the steady-state ^{1}H ^{15}N NOE experiment used a total recycle delay of 6 sec. Spectral widths of 9 kHz and 2.1 kHz in the f2 and f1 dimensions were set in all experiments, with 128 transients collected per t1 increment, and recorded as 256 complex t1 values against 1024 complex t2 values.

Exponential fitting of relaxation rates

NMR peak heights determined by the "rh" command in Sparky were used as reliable indicators of spectral intensity. The program "sparky2rate" (http://xbeams.chem.yale.edu/~loria/software.htm) read in peak intensity tables from Sparky and acted as a front-end for Curvefit (http://cpmcnet.columbia.edu/dept/gsas/biochem/labs/palmer/software.html), for exponential fitting of R_1 and R_2 NMR relaxation rates and an analysis of their associated errors using Monte Carlo simulations, which depended upon an initial error estimated from the repeated experiments. One residue was excluded from the subsequent model-free analysis (below) on the basis of poor spectral resolution (C40). Appropriately, relaxation data are not reported for prolines (residues 4, 17, 28, 41, 47, 71, 80, and 88).

Model-free analysis

ModelFree version 4.15 was used to calculate global and residue-specific motional parameters (Mandel et al. 1995). The program FAST-ModelFree (Cole and Loria 2003) automated the error analysis and model selection that otherwise requires frequent user input and intervention. An initial rotational correlation time (τ_m) was estimated from the 10% trimmed mean of the R_2/R_1 ratio. An appropriate diffusion tensor was selected by comparing the calculated optimal τ_m value and χ^2 error of simulations run under the assumption of isotropic or axially symmetric tumbling behavior. The axially symmetric condition was selected for TUG–UBL1, as there was an improvement in χ^2, more physically appropriate motional parameters, and the best-fit value for the D_{ratio} for anisotropic rotation was significantly different from unity (0.82). All model-free calculations were run with the CSA tensor set to −172 (Canet et al. 2001), a value considered appropriate for the ^{15}N spins of proteins and a backbone amide bond length of 1.00 Å, which was used by CYANA for determination of the TUG–UBL1 tertiary structure.

Electronic supplemental material

A table containing NMR relaxation parameters for the backbone amide ^{15}N nuclei along with the output of the model-free analysis is available electronically.

Acknowledgments

We acknowledge technical assistance from Mr. Syrus Meshack and critical review of the manuscript by Dr. Ya Ha. This work was supported by NIH grants R01 CA108992-01 (M.E.H.) and R21 DK070812-01 (J.S.B.); by American Diabetes Foundation grant 1-05-RA-17 (J.S.B.); and by a grant from the Charlotte Geyer Foundation (M.E.H.).

References

Alberti, S., Esser, C., and Hohfeld, J. 2003. BAG-1—A nucleotide exchange factor of Hsc70 with multiple cellular functions. *Cell Stress Chaperones* **8:** 225–231.

Bax, A., Delaglio, F., Grzesiek, S., and Vuister, G.W. 1994. Resonance assignment of methionine methyl groups and χ 3 angular information from long-range proton–carbon and carbon–carbon J correlation in a calmodulin–peptide complex. *J. Biomol. NMR* **4:** 787–797.

Bazirgan, O.A. and Hampton, R.Y. 2005. Cdc48-Ufd2-Rad23: The road less ubiquitinated? *Nat. Cell Biol.* **7:** 207–209.

Bogan, J.S., Hendon, N., McKee, A.E., Tsao, T.S., and Lodish, H.F. 2003. Functional cloning of TUG as a regulator of GLUT4 glucose transporter trafficking. *Nature* **425:** 727–733.

Bryant, N.J., Govers, R., and James, D.E. 2002. Regulated transport of the glucose transporter GLUT4. *Nat. Rev. Mol. Cell. Biol.* **3:** 267–277.

Canet, D., Barthe, P., Mutzenhardt, P., and Roumestand, C. 2001. A comprehensive analysis of multifield ^{15}N relaxation parameters in proteins: Determination of ^{15}N chemical shift anisotropies. *J. Am. Chem. Soc.* **123:** 4567–4576.

Cheetham, J.C., Smith, D.M., Aoki, K.H., Stevenson, J.L., Hoeffel, T.J., Syed, R.S., Egrie, J., and Harvey, T.S. 1998. NMR structure of human erythropoietin and a comparison with its receptor bound conformation. *Nat. Struct. Biol.* **5:** 861–866.

Cole, R. and Loria, J.P. 2003. FAST-Modelfree: A program for rapid automated analysis of solution NMR spin-relaxation data. *J. Biomol. NMR* **26:** 203–213.

Cornilescu, G., Delaglio, F., and Bax, A. 1999. Protein backbone angle restraints from searching a database for chemical shift and sequence homology. *J. Biomol. NMR* **13:** 289–302.

Delaglio, F., Grzesiek, S., Vuister, G.W., Zhu, G., Pfeifer, J., and Bax, A. 1995. Nmrpipe—A multidimensional spectral processing system based on unix pipes. *J. Biomol. NMR* **6:** 277–293.

Di Fiore, P.P., Polo, S., and Hofmann, K. 2003. When ubiquitin meets ubiquitin receptors: A signalling connection. *Nat. Rev. Mol. Cell. Biol.* **4:** 491–497.

Ding, H., Xu, Y., Chen, Q., Dai, H., Tang, Y., Wu, J., and Shi, Y. 2005. Solution structure of human SUMO-3 C47S and its binding surface for Ubc9. *Biochemistry* **44:** 2790–2799.

Dreveny, I., Pye, V.E., Beuron, F., Briggs, L.C., Isaacson, R.L., Matthews, S.J., McKeown, C., Yuan, X., Zhang, X., and Freemont, P.S. 2004. p97 and close encounters of every kind: A brief review. *Biochem. Soc. Trans.* **32:** 715–720.

Farrow, N.A., Muhandiram, R., Singer, A.U., Pascal, S.M., Kay, C.M., Gish, G., Shoelson, S.E., Pawson, T., Forman-Kay, J.D., and Kay, L.E. 1994. Backbone dynamics of a free and phosphopeptide-complexed Src homology 2 domain studied by ^{15}N NMR relaxation. *Biochemistry* **33:** 5984–6003.

Fujiwara, K., Tenno, T., Sugasawa, K., Jee, J.G., Ohki, I., Kojima, C., Tochio, H., Hiroaki, H., Hanaoka, F., and Shirakawa, M. 2004. Structure of the ubiquitin-interacting motif of S5a bound to the ubiquitin-like domain of HR23B. *J. Biol. Chem.* **279:** 4760–4767.

Funakoshi, M., Sasaki, T., Nishimoto, T., and Kobayashi, H. 2002. Budding yeast Dsk2p is a polyubiquitin-binding protein that can interact with the proteasome. *Proc. Natl. Acad. Sci.* **99:** 745–750.

Fushman, D., Ohlenschlager, O., and Ruterjans, H. 1994. Determination of the backbone mobility of ribonuclease T1 and its 2′GMP complex using molecular dynamics simulations and NMR relaxation data. *J. Biomol. Struct. Dyn.* **11:** 1377–1402.

Gao, Y.G., Song, A.X., Shi, Y.H., Chang, Y.G., Liu, S.X., Yu, Y.Z., Cao, X.T., Lin, D.H., and Hu, H.Y. 2005. Solution structure of the ubiquitin-like domain of human DC-UbP from dendritic cells. *Protein Sci.* **14:** 2044–2050.

Guntert, P. 1998. Structure calculation of biological macromolecules from NMR data. *Q. Rev. Biophys.* **31:** 145–237.

Guntert, P., Mumenthaler, C., and Wuthrich, K. 1997. Torsion angle dynamics for NMR structure calculation with the new program DYANA. *J. Mol. Biol.* **273:** 283–298.

Guterman, A. and Glickman, M.H. 2004. Deubiquitinating enzymes are IN/(trinsic to proteasome function). *Curr. Protein Pept. Sci.* **5:** 201–211.

Herrmann, T., Guntert, P., and Wuthrich, K. 2002. Protein NMR structure determination with automated NOE assignment using the new software CANDID and the torsion angle dynamics algorithm DYANA. *J. Mol. Biol.* **319:** 209–227.

Hicke, L., Schubert, H.L., and Hill, C.P. 2005. Ubiquitin-binding domains. *Nat. Rev. Mol. Cell. Biol.* **6:** 610–621.

Hipp, M.S., Raasi, S., Groettrup, M., and Schmidtke, G. 2004. NEDD8 ultimate buster-1L interacts with the ubiquitin-like protein FAT10 and accelerates its degradation. *J. Biol. Chem.* **279:** 16503–16510.

Hipp, M.S., Kalveram, B., Raasi, S., Groettrup, M., and Schmidtke, G. 2005. FAT10, a ubiquitin-independent signal for proteasomal degradation. *Mol. Cell. Biol.* **25:** 3483–3491.

Hodsdon, M.E. and Cistola, D.P. 1997. Ligand binding alters the backbone mobility of intestinal fatty acid-binding protein as monitored by ^{15}N NMR relaxation and ^{1}H exchange. *Biochemistry* **36:** 2278–2290.

Ishima, R. and Torchia, D.A. 2000. Protein dynamics from NMR. *Nat. Struct. Biol.* **7:** 740–743.

Johnson, B.A. and Blevins, R.A. 1994. NMR view—A computer-program for the visualization and analysis of NMR data. *J. Biomol. NMR* **4:** 603–614.

Kleijnen, M.F., Shih, A.H., Zhou, P., Kumar, S., Soccio, R.E., Kedersha, N.L., Gill, G., and Howley, P.M. 2000. The hPLIC proteins may provide a link between the ubiquitination machinery and the proteasome. *Mol. Cell* **6:** 409–419.

Ko, H.S., Uehara, T., Tsuruma, K., and Nomura, Y. 2004. Ubiquilin interacts with ubiquitylated proteins and proteasome through its ubiquitin-associated and ubiquitin-like domains. *FEBS Lett.* **566:** 110–114.

Koradi, R., Billeter, M., and Wuthrich, K. 1996. MOLMOL: A program for display and analysis of macromolecular structures. *J. Mol. Graph.* **14:** 51–55.

Kraulis, P.J. 1991. Molscript—A program to produce both detailed and schematic plots of protein structures. *J. Appl. Crystallogr.* **24:** 946–950.

Křižová, H., Židek, L., Stone, M.J., Novotny, M.V., and Sklenář, V. 2004. Temperature-dependent spectral density analysis applied to monitoring backbone dynamics of major urinary protein-I complexed with the pheromone 2- sec-butyl-4,5-dihydrothiazole. *J. Biomol. NMR* **28:** 369–384.

Larsen, C.N. and Wang, H. 2002. The ubiquitin superfamily: Members, features, and phylogenies. *J. Proteome Res.* **1:** 411–419.

Liu, Q., Jin, C., Liao, X., Shen, Z., Chen, D.J., and Chen, Y. 1999. The binding interface between an E2 (UBC9) and a ubiquitin homologue (UBL1). *J. Biol. Chem.* **274:** 16979–16987.

Lytle, B.L., Peterson, F.C., Qiu, S.H., Luo, M., Zhao, Q., Markley, J.L., and Volkman, B.F. 2004. Solution structure of a ubiquitin-like domain from tubulin-binding cofactor B. *J. Biol. Chem.* **279:** 46787–46793.

Mandel, A.M., Akke, M., and Palmer, A.G. 1995. Backbone dynamics of *Escherichia-coli* ribonuclease Hi—Correlations with structure and function in an active enzyme. *J. Mol. Biol.* **246:** 144–163.

Nakamura, M. and Tanigawa, Y. 2005. Noncovalent interaction of MNSFbeta, a ubiquitin-like protein, with histone 2A. *Comp. Biochem. Physiol. B Biochem. Mol. Biol.* **140:** 207–210.

Narasimhan, J., Wang, M., Fu, Z., Klein, J.M., Haas, A.L., and Kim, J.J. 2005. Crystal structure of the interferon-induced ubiquitin-like protein ISG15. *J. Biol. Chem.* **280:** 27356–27365.

Notredame, C., Higgins, D.G., and Heringa, J. 2000. T-Coffee: A novel method for fast and accurate multiple sequence alignment. *J. Mol. Biol.* **302:** 205–217.

Riley, B.E., Xu, Y., Zoghbi, H.Y., and Orr, H.T. 2004. The effects of the polyglutamine repeat protein ataxin-1 on the UbL-UBA protein A1Up. *J. Biol. Chem.* **279:** 42290–42301.

Sakata, E., Yamaguchi, Y., Kurimoto, E., Kikuchi, J., Yokoyama, S., Yamada, S., Kawahara, H., Yokosawa, H., Hattori, N., Mizuno, Y., et al. 2003. Parkin binds the Rpn10 subunit of 26S proteasomes through its ubiquitin-like domain. *EMBO Rep.* **4:** 301–306.

Schwartz, D.C. and Hochstrasser, M. 2003. A superfamily of protein tags: Ubiquitin, SUMO and related modifiers. *Trends Biochem. Sci.* **28:** 321–328.

Sharrow, S.D., Novotny, M.V., and Stone, M.J. 2003. Thermodynamic analysis of binding between mouse major urinary protein-I and the pheromone 2-sec-butyl-4,5-dihydrothiazole. *Biochemistry* **42:** 6302–6309.

Tanaka, K., Suzuki, T., Hattori, N., and Mizuno, Y. 2004a. Ubiquitin, proteasome and parkin. *Biochim. Biophys. Acta* **1695:** 235–247.

Tanaka, T., Yeh, E.T., and Kamitani, T. 2004b. NUB1-mediated targeting of the ubiquitin precursor UbC1 for its C-terminal hydrolysis. *Eur. J. Biochem.* **271:** 972–982.

Thress, K., Henzel, W., Shillinglaw, W., and Kornbluth, S. 1998. Scythe: A novel reaper-binding apoptotic regulator. *EMBO J.* **17:** 6135–6143.

Toniolo, D., Persico, M., and Alcalay, M. 1988. A "housekeeping" gene on the X chromosome encodes a protein similar to ubiquitin. *Proc. Natl. Acad. Sci.* **85:** 851–855.

van Laar, T., van der Eb, A.J., and Terleth, C. 2001. Mif1: A missing link between the unfolded protein response pathway and ER-associated protein degradation? *Curr. Protein Pept. Sci.* **2:** 169–190.

———. 2002. A role for Rad23 proteins in 26S proteasome-dependent protein degradation? *Mutat. Res.* **499:** 53–61.

Wishart, D.S. and Sykes, B.D. 1994. The ^{13}C chemical-shift index: A simple method for the identification of protein secondary structure using ^{13}C chemical-shift data. *J. Biomol. NMR* **4:** 171–180.

Wu, K., Chen, A., Tan, P., and Pan, Z.Q. 2002. The Nedd8-conjugated ROC1-CUL1 core ubiquitin ligase utilizes Nedd8 charged surface residues for efficient polyubiquitin chain assembly catalyzed by Cdc34. *J. Biol. Chem.* **277:** 516–527.

Wu, Y.H., Shih, S.F., and Lin, J.Y. 2004. Ricin triggers apoptotic morphological changes through caspase-3 cleavage of BAT3. *J. Biol. Chem.* **279:** 19264–19275.

Yu, L., Zhu, C.X., Tse-Dinh, Y.C., and Fesik, S.W. 1996. Backbone dynamics of the C-terminal domain of *Escherichia coli* topoisomerase I in the absence and presence of single-stranded DNA. *Biochemistry* **35:** 9661–9666.

Yuan, P., Marshall, V.P., Petzold, G.L., Poorman, R.A., and Stockman, B.J. 1999. Dynamics of stromelysin/inhibitor interactions studied by ^{15}N NMR relaxation measurements: Comparison of ligand binding to the S1-S3 and S′1-S′3 subsites. *J. Biomol. NMR* **15:** 55–64.

Yuan, X., Shaw, A., Zhang, X., Kondo, H., Lally, J., Freemont, P.S., and Matthews, S. 2001. Solution structure and interaction surface of the C-terminal domain from p47: A major p97-cofactor involved in SNARE disassembly. *J. Mol. Biol.* **311:** 255–263.

Yuan, X., Simpson, P., McKeown, C., Kondo, H., Uchiyama, K., Wallis, R., Dreveny, I., Keetch, C., Zhang, X., Robinson, C., et al. 2004. Structure, dynamics and interactions of p47, a major adaptor of the AAA ATPase, p97. *EMBO J.* **23:** 1463–1473.

Zhao, C., Beaudenon, S.L., Kelley, M.L., Waddell, M.B., Yuan, W., Schulman, B.A., Huibregtse, J.M., and Krug, R.M. 2004. The UbcH8 ubiquitin E2 enzyme is also the E2 enzyme for ISG15, an IFN-α/β-induced ubiquitin-like protein. *Proc. Natl. Acad. Sci.* **101:** 7578–7582.

Zuiderweg, E.R. 2002. Mapping protein–protein interactions in solution by NMR spectroscopy. *Biochemistry* **41:** 1–7.